Bennett Vorticity: A family of nonlinear Shear-Flow Stabilized Z-Pinch Equilibria

Matt Russell[1*]

Corresponding author(s). E-mail(s): russm66@uw.edu;

Abstract

Plasma equilibria are typically treated as arising from distinct mechanisms across different regimes. Here we demonstrate that a single analytic axial flow profile, obtained by exchanging the Bennett nonlinearity from density to flow, generates a family of shear-flow stabilized Z-pinch equilibria in which the properties are determined directly by the flow. This analytic profile reconstructs the axial velocity, and magnetic structure of shear-flow stabilized experiments, and reproduces the spatial structure of emission intensity in the front, wake, and needletip structures of an air plasma streamer head. Explorations of nanoscale observables illustrate both the reach and limitations of the ideal model, while the emergence of sawtooth structures when multiple of these profiles are chained together further supports its internal consistency. These results suggest that the shear flow stabilized Z-pinch equilibrium may provide a unifying framework for understanding plasma structure across disparate regimes, with potential implications for both laboratory and natural plasmas.

Keywords: Ideal MHD, Bennett Pinch, Shear-Flow Stabilized Z-Pinch, Nonlinear Science, Analytic

Introduction

Plasma equilibria across widely separated regimes are typically described using distinct physical mechanisms. Here we show that a single analytic axial flow profile generates a family of shear-flow-stabilized Z-pinch equilibria from which density, current, magnetic field, and pressure follow directly. This same profile reconstructs experimental shear-flow stabilized Z-pinch structure[1] and captures streamer dynamics, suggesting a common flow-generated origin of plasma structure across regimes.

The magnetohydrodynamic Z-pinch equilibrium is one of the chief reasons why fusion scientists, buoyed by the success of nuclear fission, predicted they would

have fusion harnessed by the end of the decade when the international community came together and declassified the field in the 50s. Unfortunately, the axisymmetric Z-pinch suffers from $m = 0$ kink, and $m = 1$ sausage instabilities which limit the device lifetime unless stabilized[2]. A means of stabilizing the Z-pinch in a manner valid for a fusion reactor was discovered about a decade or so after researchers abandoned it in a heap of bitter frustration for toroidal approaches, instead. Namely, by the means of a sheared axial flow which satisfies the criterion[3],

$$\frac{\mathrm{d}u_z}{\mathrm{d}r} > 0.1kV_A = \frac{\pi}{5L}\frac{B_\theta}{\sqrt{\rho\mu_0}} \tag{1}$$

Otherwise the axial transport of magnetic energy will be sufficient to destabilize the pinch via virulent kink and sausage MHD modes.

Theory

A Z-pinch is the simplest kind of magnetohydrodynamic equilibrium, featuring only an axial current density which creates an azimuthal magnetic field that confines the flow. With an axisymmetric system where the flow properties only depend on the radial coordinate the equations are simple enough to integrate, leaving solutions which correspond to plasma flows that in reality will collapse on nanosecond timescales unless they are shear-flow stabilized.

In the case of a high-R_m flow, where the magnetic Reynolds number is of course,

$$R_m = \mu u \sigma L \tag{2}$$

representing the relative impact of the magnetic forces against the inertial ones in a fluid of charged particles, then the governing equations are given by,

$$J_z = -en(r)u_z(r) \tag{3}$$

$$B_\theta = \frac{\mu_0}{r}\int_0^r r' J_z(r')dr' \tag{4}$$

$$\frac{\mathrm{d}p}{\mathrm{d}r} = -J_z B_\theta \tag{5}$$

The Bennett pinch is one interesting analytic solution to this equilibrium which considers a two temperature system that carries a uniform flow with a density of the form[4][5],

$$n(r) = \frac{n_0}{(1+\xi^2 r^2)^2} \tag{6}$$

$$\xi^2 = bn_0 \tag{7}$$

$$b = \frac{\mu_0 e^2 u_{z,0}^2}{8k_B(T_e + T_i)} \tag{8}$$

giving the plasma current density,

$$J_z(r) = \frac{-en_0u_{z,0}}{(1+\xi^2r^2)^2} \tag{9}$$

Let us choose to swap the profile in Equation (6) from density to flow. The flow then will entirely generate the structure of the equilibrium. In order for the momentum balance to remain consistent with the physics of the equilibrium, the temperature now must become non-uniform to compensate for the uniform density.

From the conditional in Equation (1) we can ask what is required of this non-uniform temperature in order for the flow profile,

$$u_z(r) = \frac{u_{z,0}}{(1+\xi^2r^2)^2} \tag{10}$$

to be a shear-flow stabilized Z-pinch. Derivations of the weak and strong forms that answer this question are presented in the supplemental appendix, and merely quoted here for brevity.

The weak form of the answer is,

$$T(r) > r^2 \tag{11}$$

Assuming the temperature profile to be a power-law as suggested by the above,

$$T(r) = C_T r^n \tag{12}$$

then the strong form is merely that the power of the exponent satisfies,

$$n > 2 \tag{13}$$

Inserting a cubic temperature into Equation (10),

$$T(r) = \frac{T_p}{r_p^3} r^3 \tag{14}$$

we have after some algebra,

$$u_z(r) = u_{z,0}\frac{r^2}{(r+C_{B,T}^{(3)})^2} \tag{15}$$

$$C_{B,T}^{(3)} = (1.45967 * 10^{-22})\frac{n_0u_{z,0}^2r_p^3}{T_p}\ [m] \tag{16}$$

This gives a current density,

$$J_z = -en_0u_{z,0}\frac{r^2}{(r+C_{B,T})^2} \tag{17}$$

a magnetic field,

$$B_\theta(r) = -\frac{\mu_0 e n_0 u_{z,0}}{2r(r + C_{B,T})} f(r, C_{B,T})\hat{\theta} \tag{18}$$

and a plasma pressure whose exact form is left for an appendix due to the sake of brevity. The function in the magnetic field expression illustrates the logic behind this decision as it introduces natural logarithms into the kernel for the pressure,

$$f(r, C_{B,T}) = f_1 + f_2 + f_3 + f_4 \tag{19}$$

with,

$$f_1(r) = r^3 \tag{20}$$

$$f_2(r, C_{B,T}) = -3r^2 C_{B,T} \tag{21}$$

$$f_3(r, C_{B,T}) = -6r C_{B,T}^2 (1 + \ln\left(\frac{C_{B,T}}{r + C_{B,T}}\right)) \tag{22}$$

$$f_4(r, C_{B,T}) = -6C_{B,T}^3 \ln\left(\frac{C_{B,T}}{r + C_{B,T}}\right) \tag{23}$$

Besides this "pure-flow" profile we can also add a uniform background flow to this equilibrium, as well as a sign to the shear,

$$u_z^{(2,\pm)} = u_0 \pm u_{z,0} \frac{r^2}{(r + C_{B,T})^2} \tag{24}$$

Because the current densities constructed by the above are analytic, then any combination of density and flow profile which produces one of these current densities creates exactly the same magnetic field and plasma pressure as is produced in the specific case under consideration, giving a self-similar characteristic to the system, as well as the existence of a mixed one to the fundamental character behind this result. We identify this aforementioned pureflow flow pattern with the situation when the nonlinearity is entirely distributed to the flow. Since,

$$\chi + \nu = 2 \tag{25}$$

is required if we identify these as the exponents which are distributed to the flow, and density, respectively, then $\chi = 2$ corresponds to the pureflow case.

When the bulk flow is introduced, the magnetic field picks up a term proportional to the radius, but the pressure becomes complex, and involves a Junquiere function of second order. This is noteworthy because this function typically arises in the context of quantum statistics, and this is a classical equilibrium.

The boundary conditions for the equilibrium are simple,

$$p(0) = p_0 \tag{26}$$

$$p(r_p) = 0 \tag{27}$$

$$p_0 = \int_0^{r_p} J_z B_\theta dr \tag{28}$$

$$u_z(r_p) = u_{edge} = u_{z,0} \frac{r_p^2}{(r_p + C_{B,T})^2} \tag{29}$$

but the flow boundary condition expresses a quartic system whose roots give the value of the flow speed. If the parameter, $C_{B,T}$, is small compared to the pinch radius then these values become degenerate, and only the edge speed solution remains. However, in general there will be four roots to this system, and they may be complex-valued. For brevity, the investigation of this system is found in the supplemental appendix.

The minimum pinch length that these vortices need to be shear-flow stabilized can be investigated, not just for the pureflow vortices discussed, but also for bulk vortices, and even higher-order vortices than cubic. However, the cubic vortex is the minimum energy state among this shear-flow stabilized family as the parabolic vortex has no shear, and the thermal power of an n-vortex is given by,

$$S_n = -2\pi L n \kappa T_p \tag{30}$$

with the derivation left for the appendix alongside an obtainment of the basic spatiotemporal form of the temperature perturbations from the heat equation.

The aforementioned lengths can be found straightforwardly from re-arranging the shear-flow criterion,

$$L > \frac{\pi}{5} \left(\frac{\mathrm{d}u_z}{\mathrm{d}r} \right)^{-1} V_A \tag{31}$$

Taking the limit of this expression as we approach the pinch axis, we find for the respective systems,

$$L_3^{(2)} > 0 \tag{32}$$

$$\tilde{L}_3^{(2,\pm)} > -\frac{e n_0 \mu_0 C_{B,T}^2 u_0}{4 u_{z,0}} \tag{33}$$

$$\tilde{L}_n^{(2)} > 0 \tag{34}$$

$$\tilde{L}_n^{(2,\pm)} > \lim_{r \to 0} \frac{(r^n + C_{B,T}^{(n)} r^2)^3}{r^{2n}} \tag{35}$$

The lengths for the vacuum forms are naturally zero, and the lengths for the bulk forms go to zero when the pinch radius does. The tildes represent normalizations which are described in the supplement alongside the derivation of these expressions. Evidently these vortices are all shear-flow stabilized for an arbitrarily small space. We now test whether this analytically-generated equilibrium reproduces experimentally observed plasma structure.

ZaP Reconstructions

This analytic flow profile reconstructs the axial velocity profiles observed in the shear-flow stabilized Zap Z-pinch experiments[6][1]. Either a single form of vortex can be solved for across an entire half-chord, or the solution can be localized in each cell of the experimental data using the associated speeds as boundary conditions. In doing this, the edge temperature of the system is chosen to coincide with the core temperature of the plasma. If this approach fails due to the natural limitations of the MHD model here, e.g., neglecting viscosity, kinetic effects, relativistic physics, etc.. then the parameter $C_{B,T}$, which represents the placement of the shear layer, can be tuned so that the flow rises to the edge state when it needs to. This reflects the inherent self-similarity of the model based on a physically-bound parameter, rather than an unconstrained curve-fitting exercise using a free value. Unless noted otherwise, the magnitude of the flow root is taken rather than just the real part. Consequently, the accuracy of these solutions will suffer greatly as the shear layer will be located beyond the pinch radius due to the largeness of the flow magnitude from these imaginary velocities. They arise due to the structure of the quartic equations which must be solved when obtaining the flow roots.

To evaluate the closeness of fit, the relative rate of mean squared error is calculated between the analytic solution, and linear interpolant, for the roots of each segment before these values are averaged respectively,

$$\overline{RRMSE} = \frac{1}{N_V} \sum_{i=0}^{N_V-1} \frac{\sqrt{MSE_i}}{mean(u_{lin,i})} \tag{36}$$

A cubic, pure-flow vortex will have four roots per problem unless $u_0 = u_{edge}$, in which case there will be no roots because the problem is made trivial. Tables (1) - (2) list the experimental reconstructions made, and the closeness of fit between the analytic solution expressed by a chain of given roots, and the experimental sawtooth data.

Experiment	HC	T_p (keV)	Root 1 (%)	Root 2 (%)	Root 3 (%)	Root 4 (%)
Zap 2001 (FS)	+	0.2	21.086	21.086	21.483	21.483
Zap 2001 (FS)	+	2	23.211	23.211	33.221	33.221
Zap 2001 (FS)	+	10	26.606	26.606	44.046	50.305
Zap 2001	+	0.2	8.766	8.766	5.349	5.349
Zap 2001	+	2	4.753	4.753	13.057	13.057
Zap 2001	+	10	1.565	1.565	18.249	37.433
Zap 2001 (ELV)	+	0.2	13.761	13.761	6.789	22.871
Zap 2001 (FS)	-	0.2	28.092	28.092	24.822	24.822
Zap 2001 (FS)	-	2	22.729	22.729	19.412	19.412
Zap 2001 (FS)	-	10	17.901	17.901	20.548	44.886
Zap 2001	-	0.2	22.807	22.807	19.931	19.931
Zap 2001	-	2	18.629	18.629	20.992	20.992
Zap 2001	-	10	15.284	15.284	23.051	50.271
Zap 2001 (ELV)	-	0.2	17.812	17.812	8.463	14.599

Table 1 Closeness of fit between the experimental shear-flow stabilized Z-pinch velocity data, and analytic single-vortex reconstructions for the positive (+) and negative (-) half-chords (HC) based on positive and negative bulk, pureflow vortices, respectively. The closeness is compared both on the full span, and when data points near the edge of the pinch are neglected with this latter category indicated by the absence of (FS) in the 'Experiment' field. Reconstructions that use an edge-localized vortex (ELV) to improve the fit at the shear layer are marked accordingly.

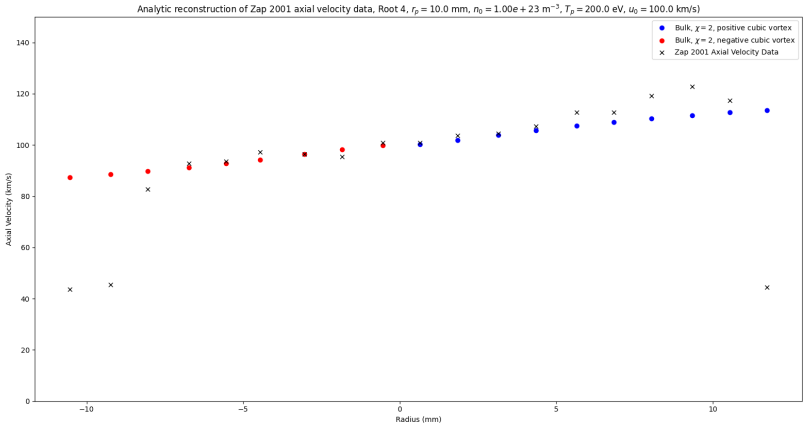

Fig. 1 Analytic, single-vortex reconstruction of the Zap 2001 experimental velocity profile based on the most accurate solution. Evidently, the shear of this solution naturally captures subtleties in the shear of the experimental profile, however, the location of the shear layer is too large in the analytic solution which is what leads to the large discrepancies seen in Table 1.

Streamer Validation

This model also reconstructs the intensity of emitted light in the head of an air plasma streamer[7]. A linear model connects the plasma current density with the

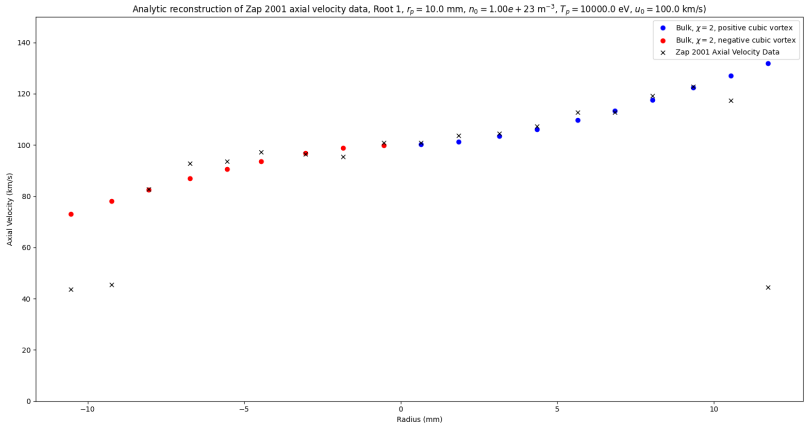

Fig. 2 Analytic, single-vortex reconstruction of the Zap 2001 experimental velocity profile based on altering the plasma properties in order to tune the location of the shear layer. This process improves the accuracy in the negative half-chord, but degrades it in the positive half-chord because the positive vortex being fit there does not model the negative shear seen in the experiment.

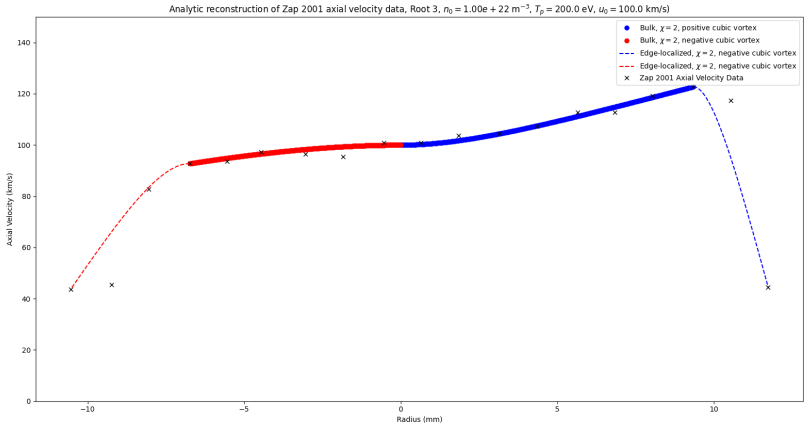

Fig. 3 Edge-localized vortex (ELV) reconstruction of the Zap 2001 experimental velocity profile based on grids with $N_r = 500$ points for each vortex. Just like with the sawteeth reconstructions of the 2009 data the third branch of solutions is the most accurate, suggesting nature has a preferred path.

emission of photons from the plasma, I,

$$I = \alpha J_z \tag{37}$$

Experiment	Shot	Root 1 (%)	Root 2 (%)	Root 3 (%)	Root 4 (%)
Zap 2009	$\tau = 29.6\ \mu s$	2.463	2.463	1.414	4.926
Zap 2009	$\tau = 38.4\ \mu s$	4.682	4.683	3.278	11.104
Zap 2009	$\tau = 41.4\ \mu s$	7.336	7.336	4.577	15.814
Zap 2009	$\tau = 48.96\ \mu s$	4.655	4.655	3.427	11.464
Zap 2009	$\tau = 58.64\ \mu s$	10.369	10.369	5.919	20.613

Table 2 Closeness of fit between the experimental shear-flow stabilized Z-pinch velocity data, and the analytic reconstructions. The average RRMSE of each reconstruction is calculated from the RRMSEs of each individual segment for each root to give these numbers.

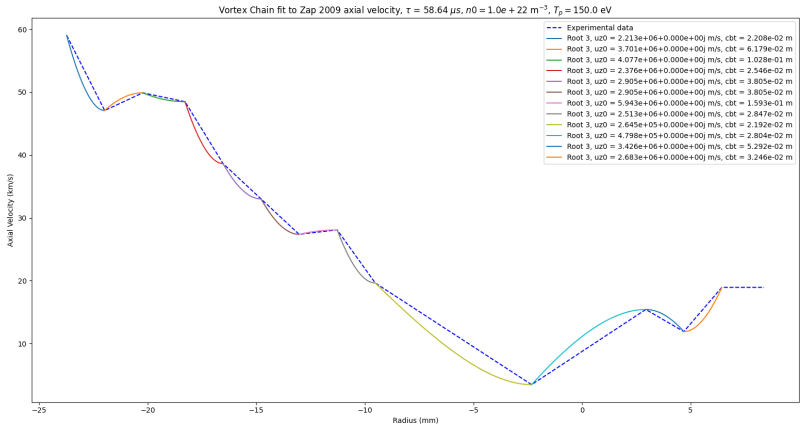

Fig. 4 Analytic reconstruction using the third solution branch for representative Zap 2009 data. The model captures the global structure measured by the experiment, and suggests a sub-grid structure to the flow.

which is justified by assuming that the primary source of photonic emission in a plasma discharge are electron-impact collisions, so that the local structure of the emission is directly related to the local electron plasma current.

The intensity falls off very rapidly in the streamer head so a range normalization is used, instead of the prior mean normalization, in the calculation of the relative mean squared error to avoid introducing an extraneous penalty. Visually, solutions to the wake, front, and needletip are presented in Figure (6). Large $C_{B,T}$ values associated with complex conjugate roots cause large deviations in some of the solutions, but what is noteworthy about this reconstruction is that it represents the axial current density as a function of axial coordinate which is interpreted as a pinch radius for the purposes of fitting this ideal MHD model to the plasma. Table (3) presents the data.

Why this is exceptionally noteworthy is because the assumptions behind this equilibrium include that of an axial symmetry. However, here we see no axial symmetry, and the flow pattern still makes an accurate fit when the shear layer is suitably

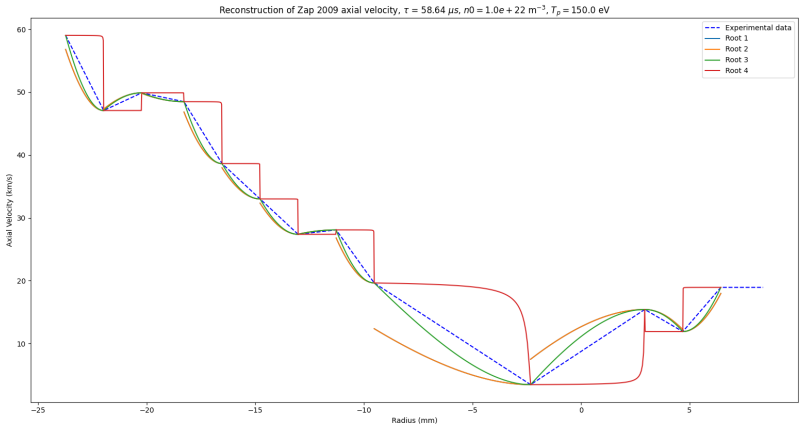

Fig. 5 Analytic reconstructions with all solution branches for the representative Zap 2009 data as in Figure (4). The first and second solution branches are identical, and possess roots which are complex conjugates of each other. The third branch naturally gives the best fit, indicating that nature has a preferred selection. This idea is supported by the data in Table (2), and these features are repeated throughout the sawtooth reconstructions.

located to match the experimental shear. This suggests that the requirement of axial symmetry can be relaxed, and supports the surprising conclusion that axial symmetry is not required for this equilibrium even though that is a fundamental mathematical assumption leading up to it.

The choice of edge plasma temperature in this is taken arbitrarily, and for a given $C_{B,T}$ that represents an accurate solution, the temperature can be tuned by varying, e.g., n_0. For example, in the wake and needletip if the density was reduced by a factor of 5, then the temperature could be as well, and the same $C_{B,T}$ would remain. With the flow constant, and pinch radius being untouched the same solution would appear, albeit with the more reasonable $T_p = 20000\ ^oK$ instead.

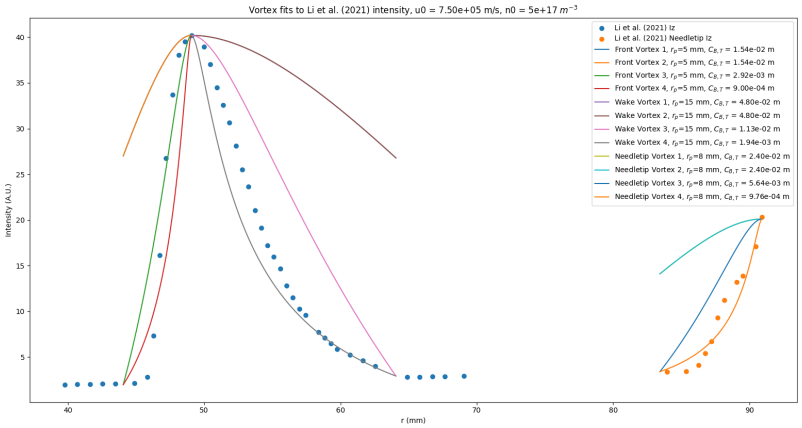

Fig. 6 Analytic single-vortex solutions to the axial intensity of an air plasma streamer viewed in the yz-plane with z interpreted as a plasma radius. The streamer front shows the same pattern as observed in many of the Zap reconstructions, namely that the third branch gives the most accurate reconstruction. However, in the wake and needletip it is the fourth branch which is the most accurate. The first and second remain complex conjugates across all three structures. The needletip can be modelled as a single vortex, but it actually appears to be comprised of two as there is a distinct form caused by a second shear layer following the rise to the edge of the first.

Structure	T_p (°K)	Root 1 (%)	Root 2 (%)	Root 3 (%)	Root 4 (%)
Front	10000	48.38	48.38	14.94	19.56
Wake	100000	54.87	54.87	21.34	10.22
Needletip	100000	55.81	55.81	23.17	8.46

Table 3 Accuracies for the analytic solutions to the air plasma streamer head structures. The mean normalization used in the Zap reconstructions is exchanged for a range normalization as the relative change in intensity is very large over a very small span so this high variance will cause the mean normalization to introduce an extraneous penalty into the accuracy. The large deviation in some of the roots results from the shear layer being located at too large a value so that the analytic vortex does not reach the edge state. This coincides with the complex conjugate roots. The large temperatures attained at the wake and needletip can be lowered by lowering n_0 while keeping the same $C_{B,T}$, and r_p so that the solutions are the same.

Applications

Because the equilibrium is entirely generated by the axial flow profile, and remains valid at arbitrarily small scales under shear-flow stabilization, this suggests that its applicability is not restricted to a specific device or regime. The scale-free nature of this equilibrium suggests broader relevance across plasma systems, from laboratory discharges to astrophysical filaments, and its inherent structure provides several novel

avenues where it can naturally be employed in a critical technological capacity beyond that of the context of magnetic fusion energy science for baseband power generation.

The list presented here is by no means claimed to be exhaustive, as this phenomena is tied to the mathematical theory of non-relativistic high-R_m MHD flows, which fusion plasmas behave similar to because they are fully-ionized, and other systems also could behave similar to, to varying degrees. Fusion plasmas also require an understanding of the relativistic theory of the equilibrium as the experimental data suggest there are significant relativistic populations[8]. The dynamics of the fast compression process at play is dominated by the growth of strong electric fields, and the presence of these is a common feature in both the fusion, and air plasma streamer head experiments.

Plasma Filament Formation

For example, we can posit that it provides a candidate mechanism for filament formation at all scales, including galactic ones. Treating a test plasma mass as fixed, we can calculate the relative impact of electromagnetic forces against gravitational forces in the pinch,

$$\eta_{GL} = \frac{\int_V |\vec{F}_G(r)| dV}{\int_V |\vec{F}_{L,lab}(r)| dV} = \frac{I_G}{I_{EM}} \tag{38}$$

In order to lift the singularity in the denominator that comes from Ohm's Law in this idealized treatment of the plasma,

$$\vec{E} = -\vec{u} \times \vec{B} \tag{39}$$

we must boost to a frame that is travelling at a velocity, $\vec{v}_{boost} = -2\vec{u}$, relative to the plasma. This calculation is involved, but can be carried out. The result is we find,

$$\eta_{GL} \sim \frac{L}{r_p} \tag{40}$$

For a relativistic flow in a flat spacetime the pinch length contracts in the flow frame to a new length, L',

$$L' = \frac{1}{\gamma(v)} L = L\sqrt{1 - \frac{v^2}{c^2}} \tag{41}$$

In the ultra-relativistic limit, $v \approx c$, this length goes to zero. Ultra-relativistic particles in this equilibrium then do not see a pinch at all as they simply "jump" to the end of it once borne. This suggests a mechanism by which the structure can form, namely, high-energy electrons which propagate on the fastest timescale in a plasma. If fast electrons were to assume the equilibrium, then the rest of the plasma will have no choice but to move collectively with them for the duration of the thermal lifetime.

High-Thrust Fusion Propulsion

If a fusing vortex plasma were to split into N distinct vortices, like is observed in the "red sprite" mesospheric discharge phenomena, then conservation of energy

suggests a mechanism for a fusion jet based on this idea to achieve high levels of thrust,

$$T = \dot{m} u_e \tag{42}$$

When the core plasma splits into a number of N distinct heads, this causes a redistribution of energy amongst the exhaust vortices which define the exhaust plane so that an adiabatic treatment of the system at the plasma edge yields,

$$\frac{1}{2} m u_{z,0}^2 + \frac{3}{2} k_B T_p = \frac{N}{2} m u_e^2 + \frac{3}{2} k_B T_e \tag{43}$$

If each exhaust vortex remains at the same edge temperature as the core vortex, then $T_e = N T_p$, and

$$u_e = \sqrt{u_{z,0}^2 - \frac{3 k_B T_p (N-1)}{m}} \tag{44}$$

If the total thermal energy in the plasma remains fixed instead, then,

$$u_e = \frac{u_{z,0}}{\sqrt{N}} \tag{45}$$

In both cases, a lowered exhaust velocity is obtained. Then we can see from the fusion jet thrust,

$$T = \frac{2 \eta_J P_{fusion}}{u_e} \tag{46}$$

that for a power-limited thruster this will result in an elevated thrust at the expense of the need for a large mass flow rate. Because of its repeating structure as a spatially periodic set of plasmas arcing through space, this system can be said to look somewhat like a plasma photonic crystal in total, and one that is a connected to a core model at its base. The entirety of the structure then can couple the equilibrium theory further to the dynamic case of the fusion red-sprite discharge process where the microscopic dynamics of each of the separate pinches twisting through space independently under the action of their magnetohydrodynamic flow. The trick then is how to get this action to produce the maximum number of exhaust vortices, which are analogous here to the needletip translating forward but as a consequence of fusion energy rather than an air plasma discharge. The scaling is also particularly poor here in the ideal case, which is a definite motivation to study the intrinsic physics of the pinch process further in order to continue to better understand the exact dynamics of the sprite transition process. Lastly, stagnation of the exhaust vortices is undesirable as it will result in the collapse of the structure as the solutions become null.

While this analysis is largely preliminary, and entirely theoretical at this point, the adiabaticity of the profile is highly suggestive of applicability to this context, as it is also to the context of baseband magnetic fusion energy. It is fair to say then that it challenges, and upends, existing scientific notions that fusion propulsion is unfeasible for a manned mission to Mars[9].

GHG Thermal Plasma Chemistry - Waterfall Reactors

By aligning the pinch axis with a uniform local gravitational field, such as found on the surface of the Earth, then strong radial plasma drifts will result because this "waterfall drift" scales inversely with cyclotron frequency,

$$\vec{v}_{wf} = \frac{g_0}{\omega_{cj}}\hat{r} \tag{47}$$

These drifts can be used in a thermal plasma reactor based on a pureflow Bennett vortex to potentially deposit ionized greenhouse gases outside of the pinch volume as the interior of these structures possesses a naturally small magnetic field (cyclotron frequency)[10]

$$\omega_{cj} = \frac{|q_j|}{m_j}B \tag{48}$$

Collisions interrupt the picture of this waterfall drift freestreaming ionized pollutants out of a shear-flow stabilized Z-pinch plasma in order to deposit them on a material surface for sequestration. If the collisionality in the plasma is low, then the transport is ballistic, and assuming perfect sticking, i.e., no reflections, the rate of mass being deposited out of a layer of the plasma is taken to be,

$$\dot{M}_s(r) = 2\pi r L m_s \Gamma_{wf}(r) \tag{49}$$

$$\Gamma_{wf}(r) = n(r)v_{wf}(r) \tag{50}$$

When the collisionality in the plasma is high, then the transport becomes diffusive, and the radial drift depends on an ordering between collision frequency and cyclotron frequency. From a force balance with a collisional drag this gives the radial drift as,

$$\vec{v}_{wf}^{(coll.)} \cdot \hat{r} = \frac{\omega_{cj} g_0}{\omega_{cj}^2 + \nu^2} \tag{51}$$

From considering the above, and the flux of mass out of the plasma due to these drifts, it is evident that there is a substantial challenge in achieving significant mass deposition. The hope is that the core of the pinch will produce fast enough particles in a small enough expanse that the timescale of their traversal will be small enough to avoid collisions. A full treatment of the problem requires studying the collisional transport of a specific configuration outside the asymptotic limits presented here. This is outside the scope of this article for reasons of brevity, and depth. The purpose of this section is to ideate an application of this technology which potentially has great technological promise in a critical field given the magnetic null on the pinch axis.

Analytic solutions for the drifts of a representative air plasma cubic vortex are shown in Figures (7) - (10) where the edge speed is taken to be a meter per second. These profiles are constructed with a value of $r_{int} = 10$ $[\mu m]$ for the minimum radius of the disc. Varying this value will change the on-axis velocity, for example, decreasing it to $r_{int} = 1$ $[\mu m]$ with the given plasma properties will lead to the presence of unphysically large (FTL) velocities for the radial drifts close to the axis. This numerical

artifact stands in contrast to the unphysically large axial, $\vec{E} \times \vec{B}$ drift velocity that remains even when the aforementioned unphysical numerical artifacts are gone.

Another interesting point to note in this data is the occurrence of the flow solutions for the first three roots, namely that they are all clustered tightly around values which are very close to the speed of sound in air. Investigating the basis for this is beyond the scope of this article, for reasons of brevity, but due to the lack of generality in the analysis it is highly suggestive for this sort of structure to appear, particularly alongside the occurrence of complex conjugates in the first two flow roots.

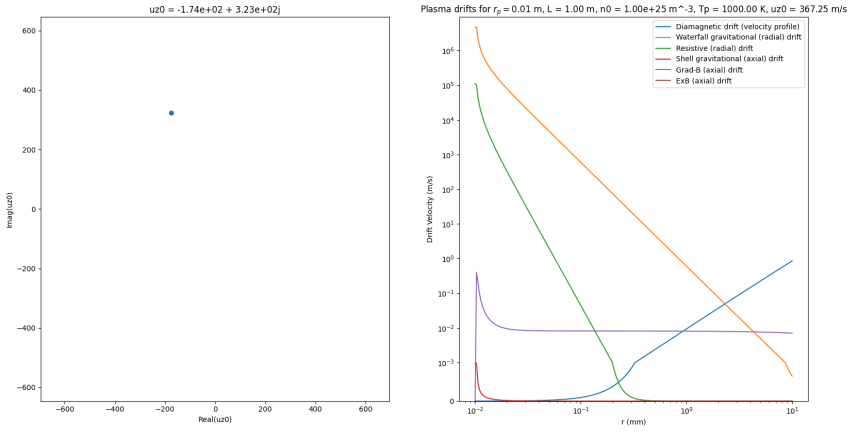

Fig. 7 The air plasma drifts for the first root of a pure-flow cubic Bennett vortex based on a meter per second edge speed, and a modest plasma temperature. Due to the similarity in computed flow speeds between the first three roots, being slightly above the speed of sound in air, for these properties the drifts are very similar in structure. Both resistive and waterfall drifts are very strong close to the axis with the plasma needing to reach close to its edge state before its flow dominates.

Deep Neural Network Neuron

The flow profile discussed in this article is also suitable for implementation as the activation function of a deep neural network. The same is true of many functions, however it is worth briefly commenting on how similar it is in structure to the 'sigmoid' function,

$$f_{sigmoid}(x) = \frac{1}{1 + \exp(-x)} \tag{52}$$

Both qualitatively, and quantatively. In fact, they are nearly identical as the normalized form of a pureflow cubic vortex can be written as,

$$f_{cpf}(x) = \frac{1}{(1 + x)^2} \tag{53}$$

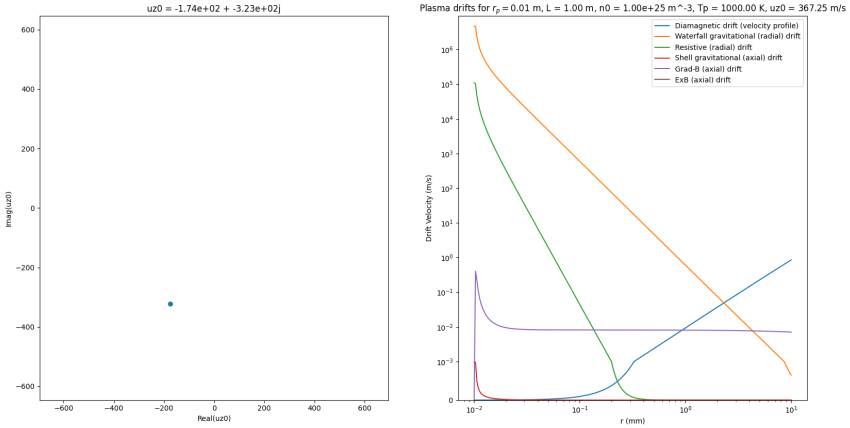

Fig. 8 The air plasma drifts for the second root of a pure-flow cubic Bennett vortex based on a meter per second edge speed, and a modest plasma temperature. Due to the similarity in computed flow speeds between the first three roots, being slightly above the speed of sound in air, for these properties the drifts are very similar in structure. Both resistive and waterfall drifts are very strong close to the axis with the plasma needing to reach close to its edge state before its flow dominates.

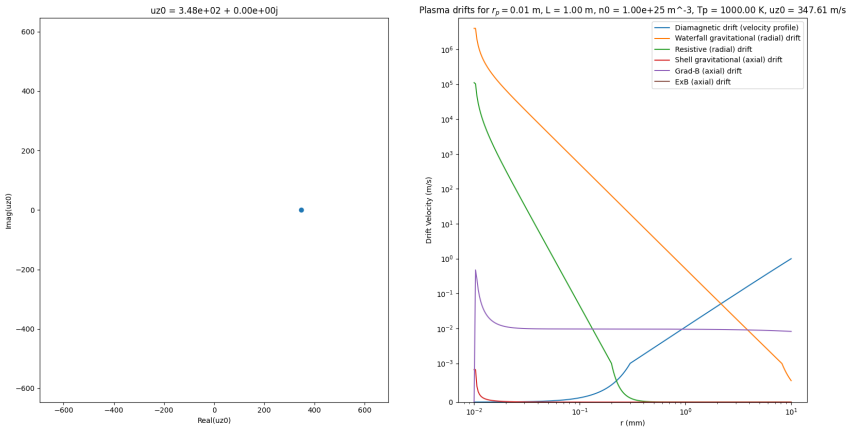

Fig. 9 The air plasma drifts for the third root of a pure-flow cubic Bennett vortex based on a meter per second edge speed, and a modest plasma temperature. Due to the similarity in computed flow speeds between the first three roots, being slightly above the speed of sound in air, for these properties the drifts are very similar in structure. Both resistive and waterfall drifts are very strong close to the axis with the plasma needing to reach close to its edge state before its flow dominates.

where $x = \frac{C_{B,T}}{r}$. The un-normalized form of a cubic pureflow vortex presents two learnable weights, the flow solution, $u_{z,0}$, and the shear layer scale parameter, $C_{B,T}$.

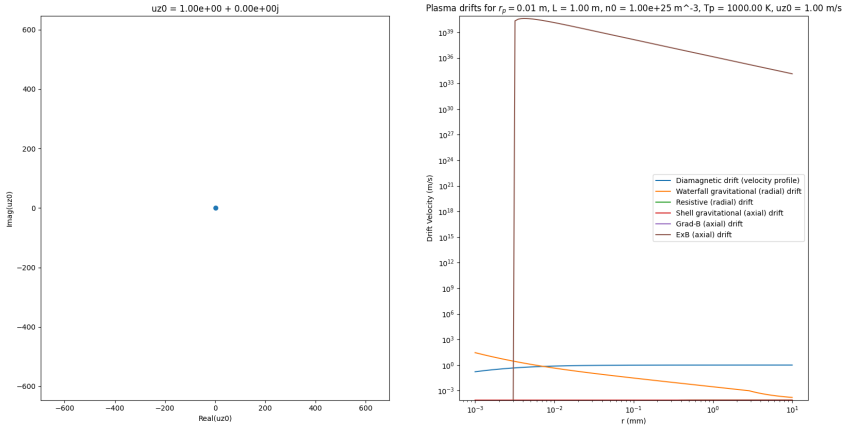

Fig. 10 The air plasma drifts for the fourth root of a pure-flow cubic Bennett vortex based on a meter per second edge speed, and a modest plasma temperature. This solution is the one where the flow constant solution is the edge speed, and what is seen is an unphysical growth in the axial ExB drift. Strictly-speaking, this is not the same thing as "electron runaway", but it is a feature which does not disappear when the interior of the plasma disc is increased, and suggests a very sudden acceleration to the plasma travelling down the axis in this solution which indicates a breaking down of the fluid theory in a regime which is kinetic as the unmagnetized core of these pinches involve betatron motion rather than that of a cyclotron.

Further discussion or analysis of this topic is outside the scope of this article for reasons of brevity as this section is meant only to briefly highlight a possible application of this research. However, as a final note on the subject, a grounded caution should be wielded when approaching the idea of treating this profile as the activation function for a DNN as it is merely a statement of fact about this profile's mathematical properties, and how they would fit in a universal function approximator, and not an ascription of any unscientific claims about its meaning.

Sawteeth

Magnetic sawteeth structures naturally arise in extended chains of this equilibrium. Unfortunately, this cannot be seen in a normalized basis,

$$\phi = \frac{r}{C_{B,T}} \tag{54}$$

because such would require the normalized pinch to be placed at a radius,

$$\phi_p = \frac{r_p}{C_{B,T}} = -\frac{1}{2} \tag{55}$$

Regardless, a positive pureflow vortex, and a negative one may be chained together before the onset of a vacuum region, and then the duty cycle of this system will regulate how far the magnetic field falls. Figures (11), and (12) illustrate this with a micrometer scale chain of vortices.

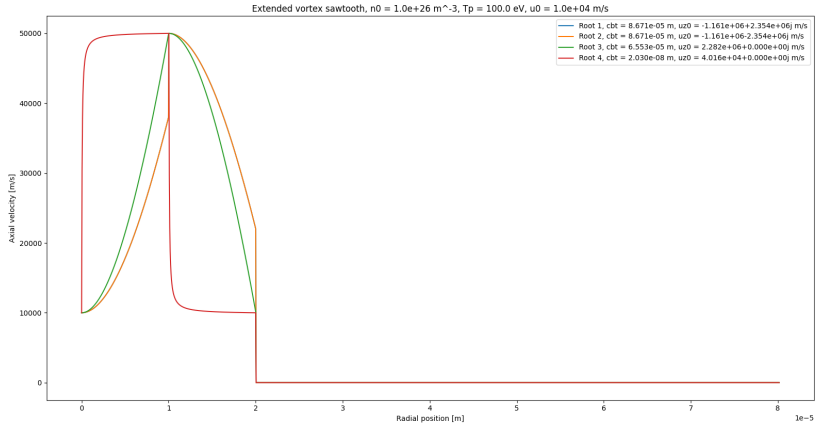

Fig. 11 Analytic solutions to a chain of microscale vortices which illustrates the natural manner in which sawteeth can arise from this form. Interestingly, we see the same pattern arise as from previous chains of multiple vortices, where the first and second roots form complex conjugates, the third root is the best fit, and the fourth has a shear layer located much closer to the axis than the other roots do.

Limitations & Discrepancies

Unphysical vortices must be neglected. For example, an electron plasma vortex with a temperature exceeding that allowed by the laws of relativity. Those remaining are understood as being an ideal construct where certain physics related to viscosity, resistivity, relativity, higher-order kinetic effects, etc.. are not incorporated. While the profile reproduces the shape of the experimental data, a large source of discrepancy arises when it does not locate the shear layer properly.

This is unsurprising as the ideal model presented here only roughly captures global features related to plasma properties supported by the 1D treatment of a shear-flow stabilized Z-pinch equilibrium. Systems that require a 2D treatment, such as a problem that considers this equilibrium in spherical coordinates, or involve mechanisms beyond the ideal treatment of a shear-flow stabilized Z-pinch, e.g., viscosity, will naturally deviate from the ideal form presented here.

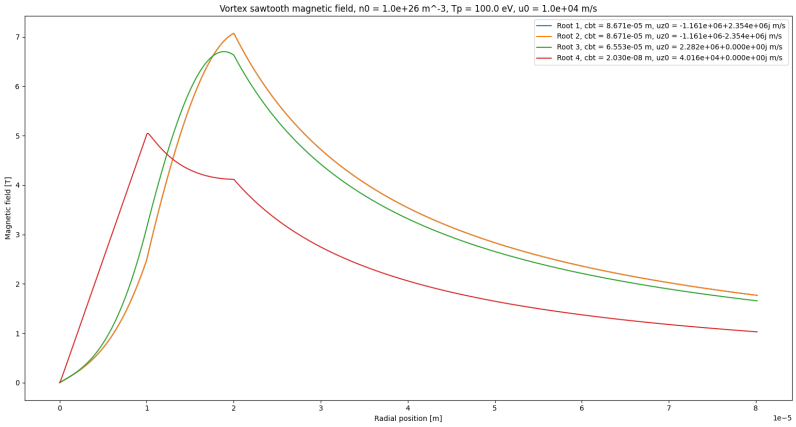

Fig. 12 Magnetic field for the microscale vortices from Figure (11) integrated with a cumulative trapezoidal routine. The lack of current in the vacuum region causes the magnetic field to fall off as $\sim \frac{1}{r}$ there so the duty cycle of this system can be tuned based on the desired falloff to the magnetic field.

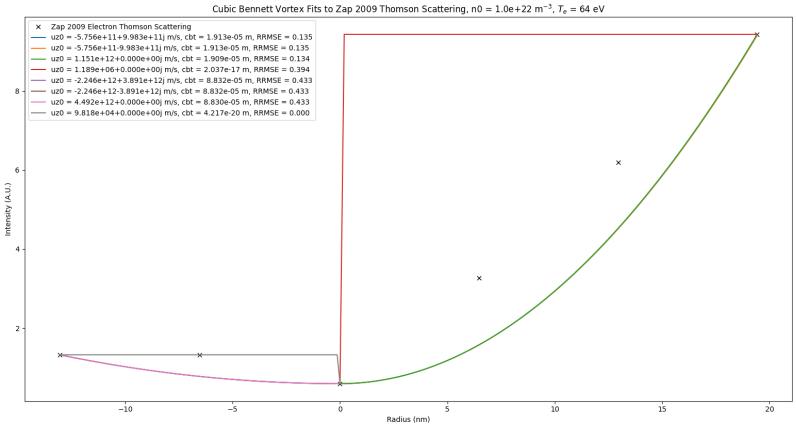

Fig. 13 Zap 2009 solutions to the nanoscale regime of Thomson scattering where the wavelength of the pulse is interpreted as a plasma radius as the ordered set of ascending wavelengths probing the plasma gives information regarding the intensity of the scattered light at successive points in the plasma. Accurate solutions to this observable here have unphysical flow velocities. Physical solutions can be seen to have shear layers around the value of the electron radius.

Discussion

The applicability of this equilibrium is evident here in a cross-regime manner, but it remains to be seen how far it extends. It arises here because the observables

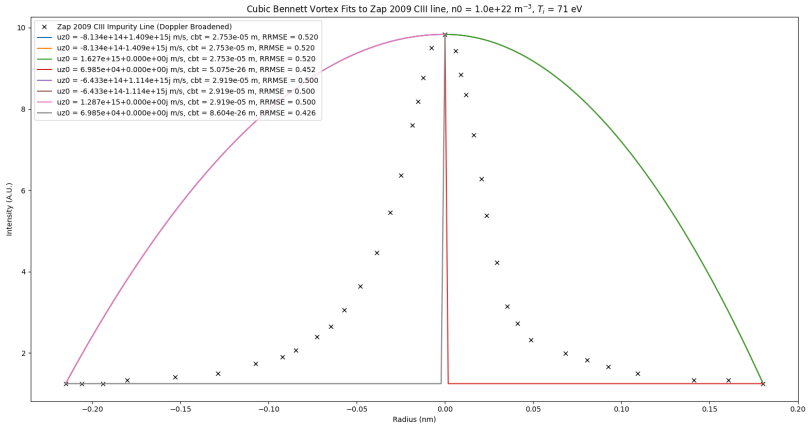

Fig. 14 Zap 2009 solutions to the sub-nanoscale regime of Ion doppler spectroscopy. The shape of the structure is a Gaussian, and vortex solutions to the ideal model either exhibit a sub-atomic scale shear layer or require unphysical flow speeds. The former leads to inaccurate solutions because the shear layer does not coincide with the observed profile, and the latter because the shear layer is larger than the interpreted pinch radius.

are a functional of current density, which is based purely on the flow as the plasma density follows from it. The flow pattern being shear-flow stabilized, and its ability to assume this form for arbitrarily small pinches, suggests that the shear-flow stabilization mechanism plays a broader role in plasma organization across multiple scales in the real world.

Acknowledgements

The author thanks Aria Johansen for constructive feedback and critical comments on the early versions of the manuscript, Sander Nijdam for discussions on the application of this equilibrium to air plasma streamer formation, Iman Datta for insightful discussions on Ideal MHD, Jack Coughlin for his feedback, Eric Meier for motivating the study of the Bennett pinch, Peter Thoreau and James Penna for their support, and Whitney Thomas for her patience.

References

[1] Shumlak, U., Adams, C.S., Blakely, J.M., Chan, B.-J., Golingo, R.P., Knecht, S.D., Nelson, B.A., Oberto, R.J., Sybouts, M.R., Vogman, G.V.: Equilibrium, flow shear and stability measurements in the Z-pinch. Nuclear Fusion **49**(7), 075039 (2009) https://doi.org/10.1088/0029-5515/49/7/075039

[2] Shumlak, U.: Z-pinch fusion. Journal of Applied Physics **127**(20), 200901 (2020) https://doi.org/10.1063/5.0004228

[3] Shumlak, U., Hartman, C.W.: Sheared flow stabilization of the $m = 1$ kink mode in Z pinches. Phys. Rev. Lett. **75**, 3285–3288 (1995) https://doi.org/10.1103/PhysRevLett.75.3285

[4] Bennett, W.H.: Magnetically self-focussing streams. Physical Review, Volume 45 (1934)

[5] Allen, J.E., Simons, L.: The bennett pinch for non-relativistic electrons. J. Plasma Phys., vol. 84 (2018)

[6] Shumlak, U., Golingo, R.P., Nelson, B.A., Den Hartog, D.J.: Evidence of stabilization in the Z-pinch. Phys. Rev. Lett. **87**, 205005 (2001) https://doi.org/10.1103/PhysRevLett.87.205005

[7] Li, X., Dijcks, S., Nijdam, S., Sun, A., Ebert, U., Teunissen, J.: Comparing simulations and experiments of positive streamers in air: steps toward model validation. Plasma Sources Science and Technology **30**(9), 095002 (2021) https://doi.org/10.1088/1361-6595/ac1b36

[8] Shumlak, U., Nelson, B.A., Claveau, E.L., Forbes, E.G., Golingo, R.P., Hughes, M.C., Oberto, R.J., Ross, M.P., Weber, T.R.: Increasing plasma parameters using sheared flow stabilization of a z-pinch. Physics of Plasmas **24**(5), 055702 (2017) https://doi.org/10.1063/1.4977468 publisher-PDF

[9] Petkow, e.a.: Comparative investigation of fusion reactions for space propulsion applications. Transactions of the Japan Society for Aeronautical and Space Sciences, Aerospace Technology Japan **7**(ists26), 59–63 (2009) https://doi.org/10.2322/tstj.7.Pb_59

[10] Crews, D.W., Meier, E.T., Shumlak, U.: Effects of transitional orbit magnetization on transport and current in z pinches. Physics of Plasmas **32**(10), 102510 (2025) https://doi.org/10.1063/5.0286743